COBEM 2023 27TH INTERNATIONAL CONGRESS OF MECHANICAL ENGENEERING

ABCM Brazilian Society of Mechanical Sciences and Engineering
27th ABCM International Congress of Mechanical Engineering
December 04-08, 2023, Florianópolis-SC, Brazil

# COB-2023-0637
# AERODYNAMIC PERFORMANCE ANALYSIS OF A PROPELLER PROJECTED FOR LOW-SPEED UNMANNED AERIAL VEHICLES

**Luís Eduardo Bispo Gonçalves**
Universidade Federal do Vale do São Francisco
luis.bispo@discente.univasf.edu.br

**Luis Francisco Dias Barreto**
Instituto Tecnológico de Aeronáutica
luisbarreto@ita.br

**José Bismark De Medeiros**
Universidade Federal do Vale do São Francisco
jose.bismark@univasf.edu.br

***Abstract.*** *This paper presents a CFD analysis of the aerodynamic performance of propellers for Unmanned Aerial Vehicles. It is worth noting that the majority of UAVs are powered by propellers, so the efficiency and effectiveness of their payloads and overall operating costs are closely linked to the performance of their propellers. Therefore, this paper seeks to describe a CFD analysis for predicting the thrust and torque of small propellers and perform experiments to determine the associated error. The technical details of a numerical simulation of a propeller using the overset mesh method on Ansys Fluent® Academic Student Release 23.1 are shown, assuming incompressible and turbulent flow conditions, constant angular velocity, and using the atmospheric conditions of Juazeiro−BA (Brazil). The procedure consists of creating the mesh for both the static and rotational domains and executing the simulation. Then, a pressure-based solution is conducted under a transient regime, and K−$\omega$ SST with curvature correction is implemented as the turbulence model based on previous works. Additionally, this study presents and discusses the experimental process implemented to validate the proposed CFD analysis. Upon comparison with the experimental results, the simulation shows a deviation of 12% in the produced thrust and an error of approximately 25% in the required torque.*

***Keywords:*** *propeller, UAV, CFD.*

## 1. INTRODUCTION

Unmanned Aerial Vehicles (UAVs) are aircraft operated without human pilots onboard. Their versatility and popularity across various industries stem from their diverse size range and applications. Propellers are essential for UAV performance, with their design impacting thrust, fuel efficiency, speed, maneuverability, and noise reduction. Computational Fluid Dynamics (CFD) analysis is crucial for optimizing propeller design, providing insights into complex fluid dynamics, and offering a cost-effective and time-efficient alternative to physical experiments.

Kutty and Rajendran (2017) aim to improve the efficiency of an advanced precision composites (APC) Slow Flyer propeller by improving airfoil selections, propeller diameters, blade angle, blade twist, and blade number. It presents a numerical method for estimating propeller performance using the software Ansys Fluent®. The results suggest that CFD simulations can significantly improve computational accuracy and provide reliable initial predictions, replacing time-consuming and expensive experimental analyses.

Pandey *et al.* (2012) and Céspedes and Lopez (2019) exhibit works that also make use of Ansys Fluent®. Pandey *et al.* (2012) analyze an isolated main helicopter rotor for hovering flight at varying rpm using Eurocopter AS350B3 blades. The goal is to determine the optimum rpm for hovering by comparing wake formations and vorticity stability. Céspedes and Lopez (2019) present the simulation and validation of a quadcopter's aerodynamic performance in hover conditions using overset mesh, which is also implemented in this paper. The simulation is conducted under incompressible conditions and K−$\omega$ SST as the turbulence model, resulting in a discrepancy of less than 7% on thrust and 22% on torque required.

Similar to the aforementioned, Lopez *et al.* (2017) and Pérez Gordillo *et al.* (2019) present CFD analyses using the turbulence model K−$\omega$ SST and comparing its results to other models and methods. Lopez *et al.* (2017) explore the use of CFD to understand the aerodynamics of UAVs, specifically the wake of a quadcopter propeller in hover. The authors use Spalart Allmaras and K−$\omega$ SST turbulence models to simulate the propeller and predict wake, thrust, and moment coefficients. The numerical results of thrust and torque were validated with flying tests, and both models predicted the correct tendency of thrust. However, the models overestimate thrust and torque by 18%. Pérez Gordillo *et al.* (2019)

investigate the performance of a quadcopter rotor operating at hover using two computational methods: CFD and the Unsteady Vortex Lattice Method (UVLM) with a viscous correction. The study uses the Multi Reference Frame model and K$-\omega$ SST turbulence model for CFD simulations and the tip vortex core growth for UVLM. Results show that UVLM overestimates the rotor's efficiency, while CFD predictions are close to experimental values.

This paper presents a CFD analysis framework using the software Ansys Fluent® under Academic Student Release 23.1, with the objective of predicting the thrust and torque generated by a small propeller. The methodology involves numerical simulations of the propeller under specific conditions, taking into account incompressible flow, turbulent effects, constant angular velocity, and local atmospheric conditions representative of Juazeiro, Bahia, Brazil. The governing equations were solved within the physical domain using the finite-volume method and the K$-\omega$ SST turbulence model. Additionally, static experiments were conducted to assess the accuracy of the predicted results. Consequently, the research's significance lies in its potential to streamline product development, reduce costs, and optimize UAV performance by improving propeller design.

## 2. METHODS

### 2.1 Computational method

#### 2.1.1 Geometry

The propeller used for this work was designed for the piston engine ASP S61 AII, Fig. 1 shows the performance data of this engine (Billinton, 1990). The definition of its geometry followed the methodology presented by Eugene Larrabee and French (1983), resulting in a powertrain with great relation between thrust and power. The propeller is made of carbon fiber and can be specified as a 0.36x0.08 meters propeller, shown in Fig. 2, indicating that the rotor has a diameter of 0.36 meters and a fixed pitch of 0.08 meters (around 3 inches).

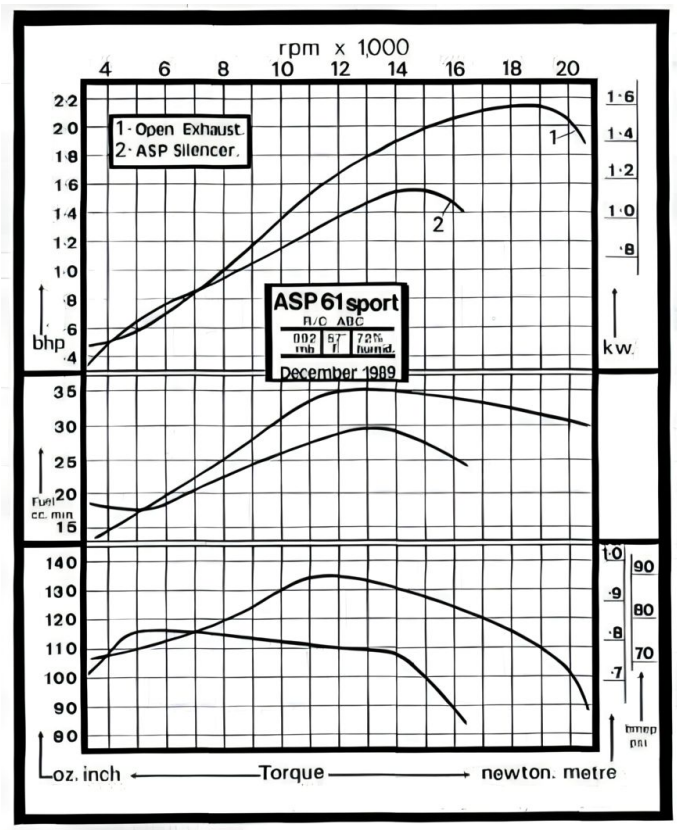


Figure 1. Power performance data of the engine ASP S61 AII (2-ASP Silencer).

#### 2.1.2 Computational domain and mesh

The computational domain and meshing methodology employed in this study were derived from the work conducted by Céspedes and Lopez (2019). Taking into account that the analysis in question is a transient study, that is, it proposes to analyze the dynamic behavior of the propeller and the flow over time, the chimera mesh method is implemented. The

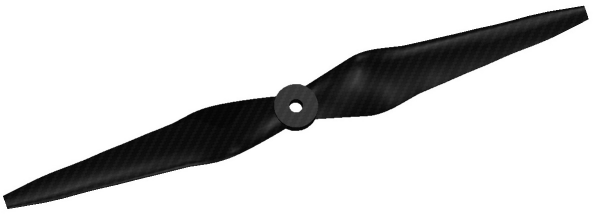

Figure 2. CAD model of the simulated propeller.

chimera methodology, also known as the overset-mesh method or overlapping meshes, involves creating independent meshes for moving objects and allowing them to overlap. The solution is calculated on the mesh near the object, obtained on a background mesh, and interpolated on the boundary between the meshes, called the overset boundary. This method offers advantages such as building meshes independently for moving objects, making meshing easier, and potentially reducing the number of elements required.

The overset region dimensions were set to be large enough to contain the boundary layer refinement. In pursuit of employing an overset mesh, the domain is divided into two regions, the first one being the rotating region (overset) and the other being a stationary region (farfield), as shown in Fig. 3.

The boundary conditions for the cylinder's upper and lateral surfaces were set to pressure inlet with a gauge pressure of 0 Pa and pressure outlet for the lower surface (gauge pressure of 0 Pa), with intermittency set at 0 and turbulent intensity at 1%, and the propeller surface modeled as a non-slip wall.

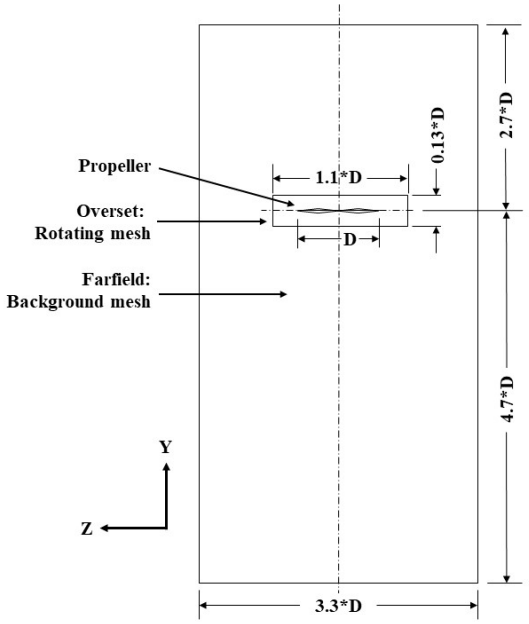


Figure 3. Representation of the computational domain.

Since the number of cells and nodes is limited due to the student license (maximum of 512 hundred elements), it was aimed to refine the regions next to the rotating zone and the blade, penalizing the regions of the far field. Thus, the mesh is unstructured and composed of tetrahedron elements with a grow rate of 1.4 to the static zone and 1.2 to the rotational region. Figure 4, 5, and 6 shows the resulting mesh containing 511 hundred elements.

Figure 5 shows the resulting mesh for the rotational domain and overset boundary, presenting an average skewness of 26.3% and an average orthogonal quality of 72.2%. In order to refine the mesh close to the edges of the propeller, the boundary layer thickness was sized considering 23.5% and 71.8% of the blade's span using flat-plate boundary layer theory presented on White (2003). Therefore, the resulting boundary layer for the 23.5% blade's span, which is thicker than the resulting at 71.8%, was divided into prisms with a grow rate of 1.4 and a size of 5.5E-6 meters for the first element, Fig. 6, such that the Y+ is 1.5 at the 71.8% blade's span region.

### 2.1.3 Atmospheric conditions

The simulation and experiment were conducted under similar atmospheric conditions of Juazeiro−BA (Brazil), with the air's density and viscosity being the only variables of concern. This was due to the nature of the problem at hand, which

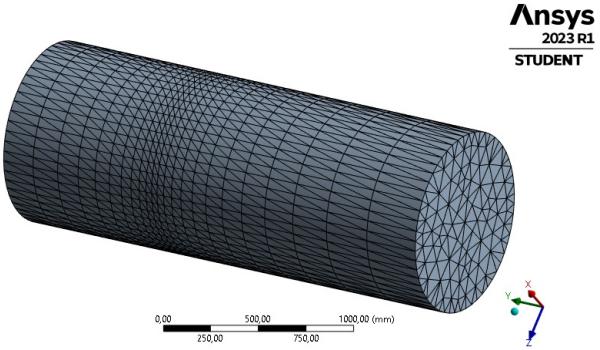


Figure 4. Resultant mesh of the stationary region.

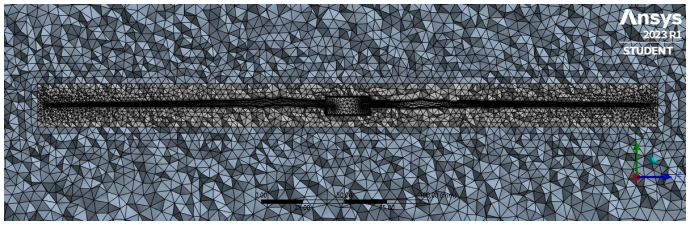


Figure 5. Resultant mesh of the rotational region with overset boundary and the mesh transition to the farfield.

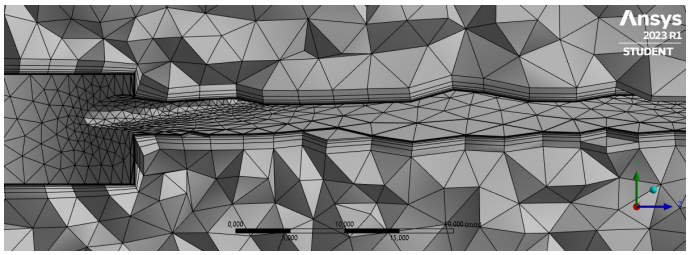


Figure 6. Orthogonal mesh refinement on the propeller surface.

required a specific regime to be established. The BMP280 sensor was used to measure the air pressure and temperature in order to obtain atmospheric condition data for the experiments. Thus, the density can be calculated by Eq. (1) derived from the ideal gas equation and viscosity calculated with Sutherland (1893) law, Eq. (2).

$$\rho = \frac{P}{R \times T} \quad \left[\frac{kg}{m^3}\right], \tag{1}$$

$$\mu = \frac{1.458 \times 10^{-6} \times T^{3/2}}{T + 110.4} \quad \left[\frac{kg}{m.s}\right], \tag{2}$$

where $\rho$, $\mu$, $P$, $R$, and $T$ are air density, air viscosity, local pressure in Pascal, specific gas constant for air in J/(kg·K), and local temperature in Kelvin, respectively. Hence, for the case presented in this work, the air density and viscosity values are 1.115 kg/m$^3$ and 1.860E-05 kg/ms.

### 2.1.4 Solution

Under a transient regime, a fully turbulent pressure-based solution is applied using a constant angular velocity of 12500 rpm to the propeller. The pressure-based solution is achieved through the application of the Navier-Stokes equations, which describe the motion of fluid particles in a three-dimensional space. The transient regime allows for the analysis of time-dependent phenomena, i.e., changes in flow rate over time. It is important to indicate that the tip of the blade works with a Mach number of 0.69, a condition for which compressibility effects are relevant. However, the solution assumes incompressible flow conditions. This ensures that the density of the fluid remains constant throughout the simulation, aiming to reduce complexity, computational cost, and mesh refinement.

The turbulence model K$-\omega$ SST is implemented in this simulation, based on similar works (Céspedes and Lopez, 2019) (Nathanael *et al.*, 2021) (Devolder *et al.*, 2017) (Cerny and Breitsamter, 2020), coupled with curvature correction and a production limiter. The curvature correction is an adjustment made to the turbulence model to take into account the

effects of streamlined curvature on flow behavior. It is applied to the production term of the turbulence model to enhance its predictive capability (Zorn, 2022). While the term "production limiter" refers to a mechanism used in the equations for the turbulence model that regulates the production of turbulent kinetic energy, the turbulence model equations incorporate production limiters to ensure precise predictions of turbulent flow phenomena (Hussain, 2019). Therefore, the inclusion of production limiters is essential for obtaining trustworthy and accurate results. These limiters ensure that the turbulent model effectively captures turbulence behavior and prevents unrealistic predictions in regions where turbulence is not well-developed.

The simulation utilized a coupled scheme with a pressure-velocity solver, space discretization using a second-order upwind for momentum, turbulent kinetic energy, and specific dissipation rate, a second-order for pressure, a least squares cell-based method for gradient, and a first-order implicit for time discretization.

A hybrid initialization was selected to ensure a stable simulation. The solution was executed with a fixed time step size of 0.00025 seconds and 30 iterations per time step. The solution stabilization process required approximately 250 time steps, during which a thrust variation of less than 5% was maintained between each time step. It's worth noting that the residuals, specifically MAX residuals, were consistently below 1E-3, indicating qualitative convergence. At the end of each time step, the residuals for continuity and turbulent dissipation were less than 1E-3 and 1E-4, respectively, while the residuals for velocities and turbulent kinetic energy were less than 1E-5.

### 2.2 Experimental method

The experimental setup measures thrust and torque simultaneously using a aluminum-alloy straight bar load cell (TAL220) and an optical tachometer (POL-19) measures angular velocity independently. The instruments are placed on the support presented on Fig. 7. The process involves setting angular velocity, waiting for stabilization, and measuring torque, thrust, and angular velocity for a few seconds. Thus, the average experimental result is then obtained.

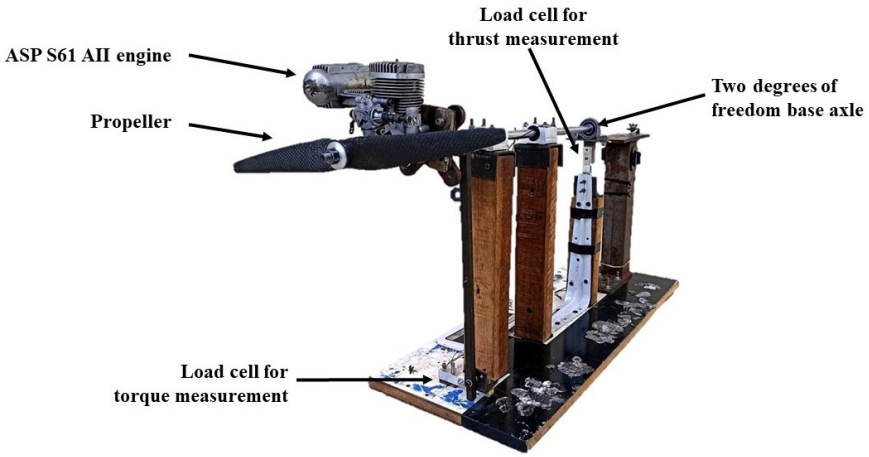


Figure 7. Experimental setup and its instruments used for thrust and torque measures. During the angular velocity setting process, the optical tachometer was supported manually.

## 3. RESULTS AND COMMENTARIES

The numerical results are divided into two categories: first, the results of field variables such as vorticity field, velocity distribution, and pressure distribution along the rotor surface are illustrated and analyzed. After that, integral variables such as thrust and torque are estimated and compared to the collected experimental data to validate the quality of the simulation data.

Figure 8 displays the Y+ contours for the upper surface of the propeller. These contours reveal that the Y+ distribution reaches its peak in close proximity to the surface, particularly in areas where the flow velocity is highest. Notably, the Y+ values are highest at the blade tips, although they consistently remain below 3. These findings align with the predictions made during the design of the meshes.

The pressure contour depicted in Fig. 9 shows a distinct difference between the pressure on the front and back sides of the propeller blade. In particular, the pressure on the back side is slightly higher than on the front side. This pressure differential works similarly to the principle used in aircraft wings, in which the pressure difference between the upper and lower surfaces generates lift force. In the case of the propeller, the pressure difference between its front and back surfaces generates a force that propels it forward, which is consistent with the results reported by Kutty and Rajendran (2017).

Figure 10 shows the far field velocity contour, the velocity behind the propeller is high, which is consistent with the

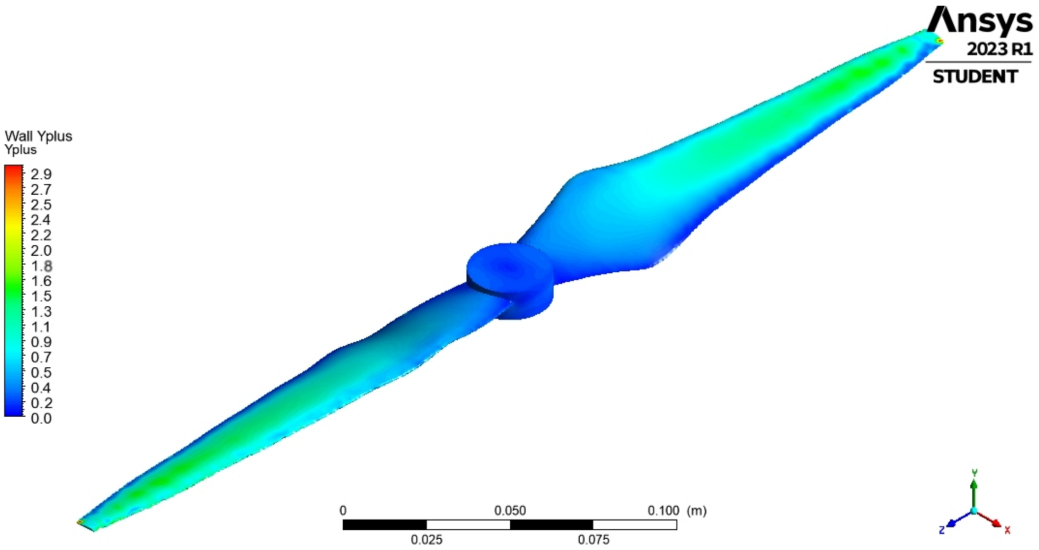


Figure 8. Y+ distribution on the propeller surface during the last simulation time step.

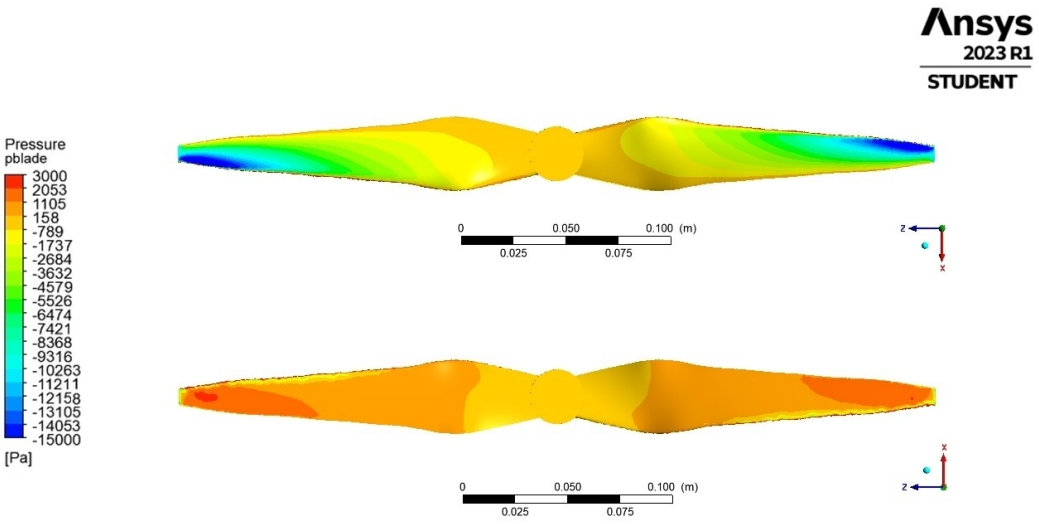


Figure 9. Pressure contour of the propeller blade. (Top) The propeller's front side; (Bottom) The propeller's back side.

theory of propeller propulsion. The velocity contour also reveals the presence of a wake behind the propeller, which is characterized by lower velocities and vortices. The higher air velocity behind a propeller is primarily due to aerodynamic forces generated by rotating blades. Rotating propeller blades create a pressure difference, as mentioned before, causing lower pressure in front and higher pressure behind it. The increased air velocity on the back side causes a region of lower pressure, causing faster flow behind the propeller. Additionally, the propeller blade's rotation generates a swirling motion, contributing to the increased air velocity.

A significant physical aspect that has been predicted is the formation of vortices. As mentioned by Céspedes and Lopez (2019), there are two important vortices, which can be identified in Fig. 11. Firstly, there is a vortex generated near the tip of each blade, which is directed downward and commonly known as the tip vortex. Secondly, there is another vortex responsible for the rotation within the wake. In the CFD results, the Q-criterion is employed to visualize the wake produced by the rotor. It is important to note that the displayed Q-criterion field is derived from the vorticity field observed from a non-inertial reference frame. Thus, Figure 11 provides a visual representation of the generated wake. An isosurface representing the Q-criterion is displayed, where the color on the surface corresponds to the magnitude of velocity measured in meters per second.

The table 1 presents the comparison between the simulated and experimental results. The order of the calculated error does not deviate from similar works, e.g., Céspedes and Lopez (2019) reported an error of 7% on thrust and 22% on torque. Thus, the simulation results show a good agreement with the experimental data, indicating that the CFD analysis

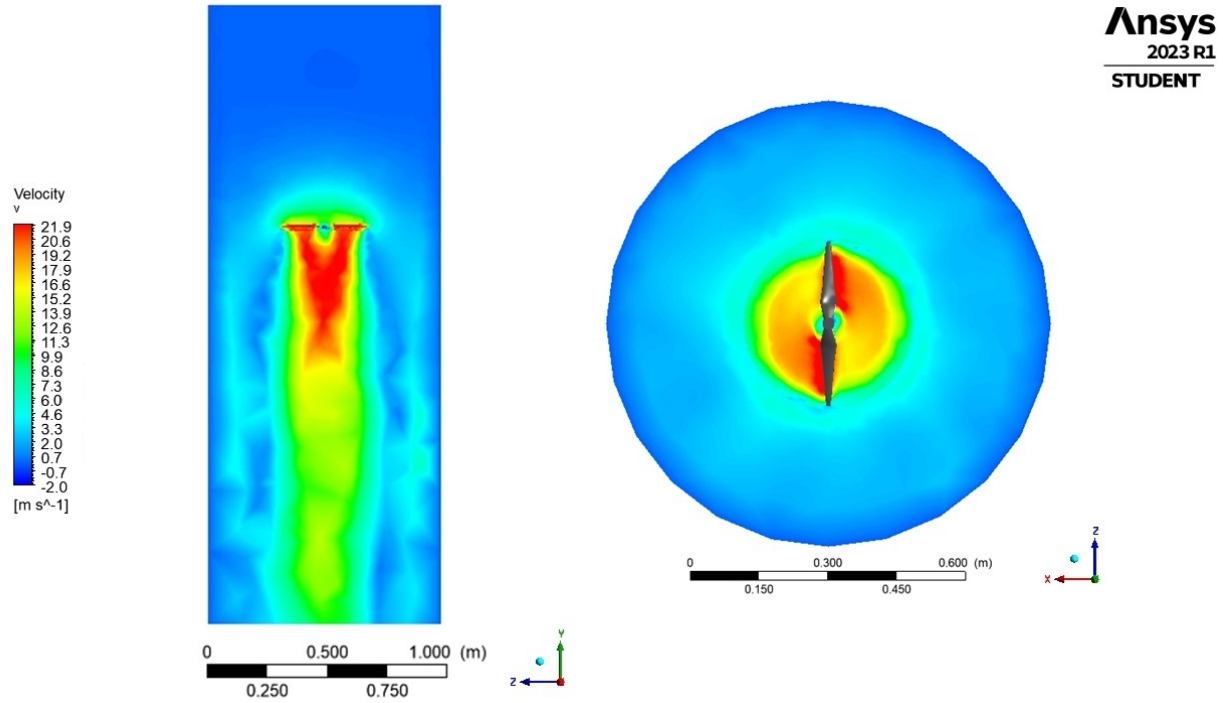


Figure 10. Velocity contour profile. (Left) Vertical cross-section; (Right) Horizontal cross-section close to and below the propeller.

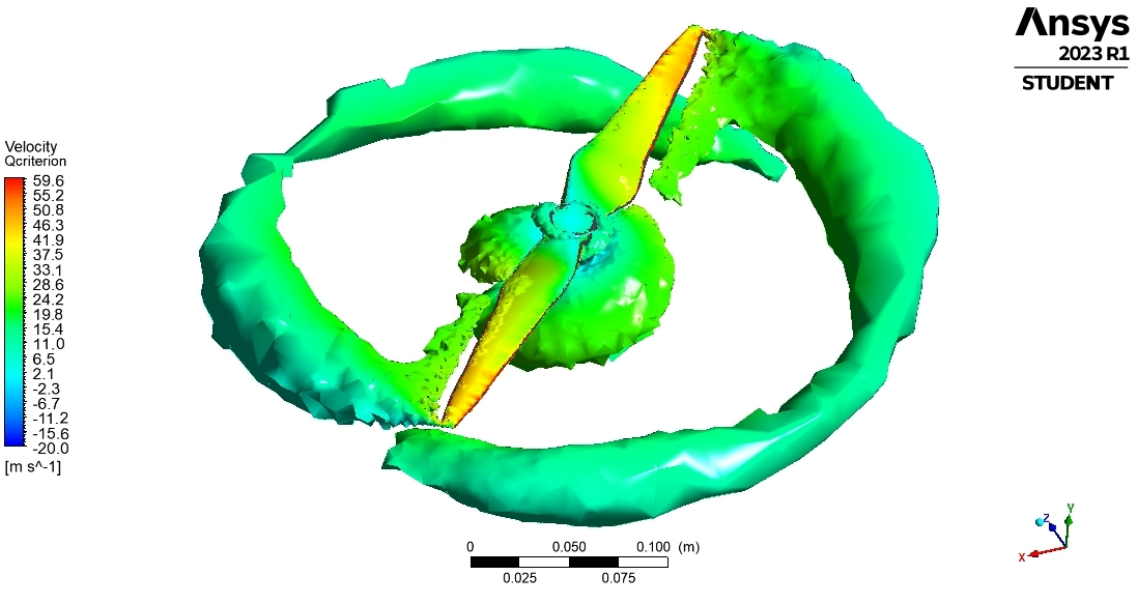


Figure 11. Vortices predicted with the simulation with Q-criterion equal to 13000 $s^{-2}$.

described in this paper is accurate and reliable, providing a foundation for further similar research. Additionally, the framework can be used to predict the behavior of similar systems under different conditions, which can be useful for optimizing their performance.

Table 1. Comparison of simulated thrust and torque values with collected experimental data.

| | **Simulation** | **Experimental** | **Error [%]** |
|---|---|---|---|
| **Thrust [N]** | 46.144 | 41.200 | 12 |
| **Torque [N.m]** | 0.855 | 0.684 | 25 |

## 4. CONCLUSIONS

This work presents a CFD analysis for predicting the thrust and torque of small propellers. The study also includes an account and analysis of the experimental process employed to validate the proposed simulation. The purpose of this validation is to assess the reliability and accuracy of the computational predictions by comparing them with the actual experimental results obtained in real-world scenarios. The paper predicts the formation of vortices and provides a visual representation of the generated wake. The simulation shows a deviation of 12% in the produced thrust and an error of approximately 25% in the required torque when compared to the experimental results.

## 5. REFERENCES

Billinton, M., 1990. "Model engine tests asp 61 (2)". Sceptre Flight, http://sceptreflight.com/Model%20Engine%20Tests/ASP%2061%20%282%29.html. Accessed: 06 Jun 2022.

Cerny, M. and Breitsamter, C., 2020. "Investigation of small-scale propellers under non-axial inflow conditions". *Aerospace Science and Technology*, Vol. 106, p. 106048. ISSN 1270-9638. doi: https://doi.org/10.1016/j.ast.2020.106048.

Céspedes, J.F. and Lopez, O.D., 2019. "Simulation and validation of the aerodynamic performance of a quadcopter in hover condition using overset mesh". *AIAA Aviation 2019 Forum*. doi:10.2514/6.2019-2824.

Devolder, B., Rauwoens, P. and Troch, P., 2017. "Application of a buoyancy-modified k- sst turbulence model to simulate wave run-up around a monopile subjected to regular waves using openfoam®". *Coastal Engineering*, Vol. 125, pp. 81–94. ISSN 0378-3839. doi:https://doi.org/10.1016/j.coastaleng.2017.04.004.

Eugene Larrabee, E. and French, S.E., 1983. "Minimum induced loss windmills and propellers". *Journal of Wind Engineering and Industrial Aerodynamics*, Vol. 15, No. 1, pp. 317–327. ISSN 0167-6105. doi: https://doi.org/10.1016/0167-6105(83)90201-5.

Hussain, S., L.J.W.L.S.B., 2019. "Thermal performance enhancement in a wedge duct with in-line pin fins combined with vortex generators". *HFF*, Vol. 29, pp. 2545–2565. doi:10.1108/hff-08-2018-0455.

Kutty, H.A. and Rajendran, P., 2017. "3d cfd simulation and experimental validation of small apc slow flyer propeller blade". *Aerospace*, Vol. 4, No. 1. ISSN 2226-4310. doi:10.3390/aerospace4010010.

Lopez, O.D., Escobar, J.A. and Pérez, A.M., 2017. "Computational study of the wake of a quadcopter propeller in hover". In *23rd AIAA Computational Fluid Dynamics Conference*. doi:10.2514/6.2017-3961.

Nathanael, J.C., Wang, C.H.J. and Low, K.H., 2021. "Preliminary investigation of wake vortex generated by spinning quadrotor propellers using overset mesh". *AIAA Scitech 2021 Forum*. doi:10.2514/6.2021-1309.

Pandey, K.M., Kumar, U., Kumar, G., Deka, D., Das, D. and Surana, A., 2012. "CFD Analysis of an Isolated Main Helicopter Rotor for a Hovering Flight at Varying RPM". Vol. Volume 1: Advances in Aerospace Technology, pp. 543–551. doi:10.1115/IMECE2012-89227.

Pérez Gordillo, A.M., Villegas Santos, J.S., Lopez Mejia, O.D., Suárez Collazos, L.J. and Escobar, J.A., 2019. "Numerical and experimental estimation of the efficiency of a quadcopter rotor operating at hover". *Energies*, Vol. 12, No. 2. ISSN 1996-1073. doi:10.3390/en12020261.

Sutherland, W., 1893. "The viscosity of gases and molecular force". *Philosophical Magazine Series 1*, Vol. 36, pp. 507–531.

White, F., 2003. *Fluid Mechanics*. McGraw-Hill international editions. McGraw-Hill. ISBN 9780072402179.

Zorn, M., K.K.R.S., 2022. "Towards accurate numerical fluid dynamics of pump-turbine runners in deep partial load operation". *IOP Conf. Ser.: Earth Environ. Sci.*, Vol. 1079, p. 012086. doi:10.1088/1755-1315/1079/1/012086.

## 6. RESPONSIBILITY NOTICE

The authors are solely responsible for the printed material included in this paper.